Confinement Effects on the Ionic Liquid Dynamics in Ionosilica Ionogels: Impact of the Ionosilica Nature and the Host/Guest Ratio

Nicole Abdou, Bruno Alonso, Nicolas Brun, Sabine Devautour-Vinot, Matthieu Paillet, Perine Landois, Ahmad Mehdi, Peter Hesemann

HAL Id: hal-03906268
https://hal.umontpellier.fr/hal-03906268v1

Submitted on 19 Dec 2022

Confinement Effects on the Ionic Liquid Dynamics in Ionosilica Ionogels: Impact of the Ionosilica Nature and the Host/Guest Ratio

Nicole Abdou[a], Bruno Alonso[a], Nicolas Brun[a], Sabine Devautour Vinot[a], Matthieu Paillet[b], Perine Landois[b], Ahmad Mehdi[a], Peter Hesemann[a]*.

[a]ICGM, Univ Montpellier, CNRS, ENSCM, 34000 Montpellier, France.

[b]Laboratoire Charles Coulomb (L2C), Univ Montpellier, CNRS, 34000 Montpellier, France.

corresponding author: peter.hesemann@umontpellier.fr

Keywords

Graphical abstract

$\sigma_{dc}^{333K} of\ TS_3^{IL}$
$= 2.88\ x\ 10^{-5}\ S.cm^{-1}$

$\sigma_{dc}^{333K} of\ TS_3^{IL}$
$= 2.23\ x\ 10^{-7}\ S.cm^{-1}$

$\sigma_{dc}^{333K} of\ TS_3^{IL}$
$= 7.07\ x\ 10^{-8}\ S.cm^{-1}$

Increase of the matrix crosslinking

Increase of the IL dynamics
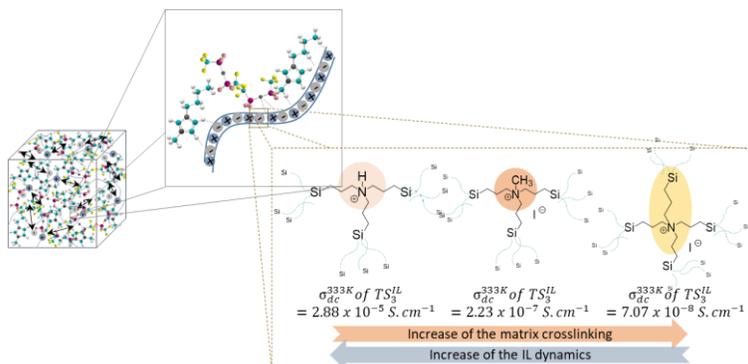
ABSTRACT

Ionosilica ionogels have been lately introduced as *emerging all-ionic designer* materials. They consist of an ionic liquid (IL) guest trapped within a solid ionosilica support host. In this work, we investigate the influence of the (*i*) ionosilica nature and (*ii*) the ionosilica/IL ratio on the mobility of the confined IL. We report the elaboration of various ionosilica ionogels *via* a nonhydrolytic sol-gel process, using namely *tris(3-(trimethoxysilyl)propyl)amine* (**TTA**), *Methyl-tris*(3-*(trimethoxysilyl)propyl)ammonium iodide* (**MTTA**) and *tetrakis(3-(trimethoxysilyl)-propyl)ammonium iodide* (**TKTA**) as ionosilica precursors, with the IL butyl-methyl imidazolium bis-triflimide (**[BMIM] TFSI**). Various ionogels were prepared from different ratios between the ionosilica host and the IL guest. The host/guest interactions *i.e.* the change in the conformational contribution of the IL counter-anion were explored by means of Raman spectroscopy. In addition, the transport properties of the confined species were probed *via* spin echo solid-state NMR experiments and Complex Impedance Spectroscopy (CIS) measurements. Raman experiments revealed different conformational equilibrium for the TFSI anion in the various ionosilica ionogels, with an increase in the *cisoid* form compared to the bulk IL due to confinement effects. The TFSI anion seems to experience different degree of confinement and thus different interactions with the ionosilica scaffold as a function of the investigated parameters. Concomitantly, the ^{1}H spin echo NMR and CIS measurements revealed a significantly higher ionic mobility in the materials synthesized in the presence of the *tris*-trialkoxysilylated ammonium precursor compared to the one synthesized in the presence of tetra-trialkoxysilylated ammonium precursor. These results may reflect stronger host-guest interactions in the latter case related to the higher degree of reticulation of the network. All these

techniques give concordant results and highlight an effect of the chemical constitution of the

ionosilica scaffold and the amount of confined IL on its dynamics within the network.

Introduction

Ionic liquids (ILs) are salts displaying melting temperatures lower than 100 °C. Due to their purely ionic constitution, ILs display unique physical and physico-chemical properties such as high ion conductivities over large temperature ranges (including very low temperatures), large liquidus ranges, low flammability, and high electrochemical stability. ILs have been subject of intense research and found applications in various areas, *e.g.* energy storage,[1] catalysis,[2-3] gas adsorption[4] and so on. The advantageous properties of ILs have recently opened the route toward commercial applications in various technologies.[5]

One of the key characteristics of ILs is their liquid state at room temperature or slightly above. This feature makes the integration of ILs in devices like batteries or membranes challenging. One solution to solve this problem is the use of ionogels (IGs) rather than pure ILs.[6] Ionogels consist of ionic liquids that are confined in a solid host matrix, with the principal aim to confer to the material the physico-chemical properties of the pure IL while modulating favorably its mechanical properties.[7] Ionogels are currently considered as a particularly innovative class of functional composite materials,[8] with high flexibility to tune their mechanical, morphological, textural, electrical, … properties.

The characteristics of ionogels are principally governed by two parameters: (*i*) the nature of the IL guest and (*ii*) the characteristics of the host matrix. Whereas a large diversity of ILs exist and can directly be implemented in ionogels' formation, the design of a suitable scaffold also affects strongly the properties of the entire system. It appears crucial to design scaffold materials that interact favorably with the IL guest in order to improve the overall properties of the resulting composites, for example in view of an enhancement of their ionic conductivity in the area of energy storage materials.[9]

In this context, ionosilicas, *i.e.*, silica hybrid materials constituted of ionic building blocks, appeared as a particularly promising class of host materials for IL confinement. Ionosilicas combine the morphological and textural polyvalence of silica with the chemical versatility of ionic liquids. They can be obtained in a large variety of morphologies such as powders, monoliths and nanoparticles,[10-12] and additionally display a high chemical polyvalence due to the presence of covalently immobilized ionic groups. So far, we particularly focused on applications of ionosilicas in separation and extraction, as for example in anion exchange,[13-15] where ionosilicas display high affinities toward various types of anionic species such as oxo-anions, drugs and dyes, but also towards biopolymers such as siRNA.[16-18] Furthermore, ionosilicas are a highly polyvalent class of materials that can be obtained from various ionosilica precursors,[19] and the interface properties of ionosilicas can efficiently be tuned both *via* the anion and the cation, resulting in a remarkable diversity of materials with tunable interface properties.[20]

More recently, we used ionosilicas as host matrix to immobilize ILs.[21] Silica based ionogels could be obtained in highly straightforward one step procedures *via* non-hydrolytic synthesis strategies starting from ionosilica precursors in IL media, in the presence of formic acid.[22-25] We applied this synthesis strategy for the formation of all-ionic composites starting from silylated ionic precursors. In these ionosilica ionogels, particular confinement effects could be observed between the ionic host matrix and IL host, highlighting the outstanding appeal of ionosilicas for the design of IL-containing composites. As an example, ionosilica ionogels can contain up to 80 wt.-% of IL while maintaining a mechanically robust and self-standing morphology. Besides this purely quantitative aspect, we could hereby show that the chemical nature of the support is of considerable significance for the elaboration of composite materials with tailored properties. We therefore took benefit of the high versatility of ionosilicas, allowing an efficient control of

texture, architecture and chemical constitution of the host material, in order to optimize the properties of the resulting ionosilica ionogel.

In this work, we explore the influence of the constitution of the ionosilica precursor and thus the nature of the ionosilica matrix on the dynamics of the confined IL [BMIM]TFSI. Therefore, three different ionosilica precursors were used for the elaboration of ionosilica ionogels using different ionosilica/IL ratios. We investigate host-guest interactions *via* the determination of the conformational change of the TFSI anion in the various ionosilica ionogels *via* Raman spectroscopy experiments. ^{1}H solid-state NMR and Complex Impedance Spectroscopy experiments elucidate the IL dynamics upon confinement. Altogether, these analyses reveal a crucial dependence between the nature of the ionosilica scaffold, the ionosilica/IL ratio and the IL dynamics. The obtained results highlight an efficient control and tuning of the ionic transport properties of ionosilica ionogel materials that can be of high interest in energy storage domains.

Experimental section

The ionosilica precursors *tris(3-(trimethoxysilyl)propyl)amine* (**TTA**), *Methyl-tris*(3-*(trimethoxysilyl)propyl)ammonium iodide* (**MTTA**) and *Tetrakis(3-(trimethoxysilyl)propyl)ammonium iodide* (**TKTA**) (figure 1) were synthesized following previously described protocols.[26] 1-Butyl-3-methylimidazolium bis(trifluoromethylsulfonyl)imide (**[BMIM]TFSI**) was purchased from IoLiTec. Formic acid (p.a.) was purchased from VWR. All chemicals were used as received.
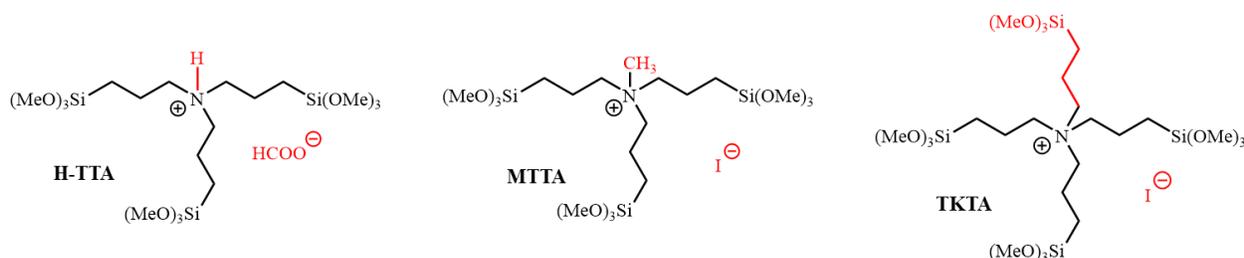
Figure 1 Molecular structures of the three ionosilica precursors *tris(3-(trimethoxysilyl)propyl)-amine* (**TTA**), *methyl-tris*(3-*(trimethoxysilyl)propyl)ammonium iodide* (**MTTA**) and *tetrakis(3-(trimethoxysilyl)propyl)ammonium iodide* (**TKTA**). Note that the protonation of the TTA precursor occurs during the synthesis of the ionosilica ionogels in the presence of formic acid, yielding **H-TTA** as represented above.

The synthesis of various ionosilica ionogels was performed in one-pot synthesis involving ionosilica precursor, formic acid and the IL. The ionosilica matrices were formed *via* non-hydrolytic sol-gel procedure from the trialcoxysilylated amine precursors in the presence of IL. First, the ionosilica precursor was mixed and vigorously stirred for three minutes with [BMIM]TFSI in a Pyrex glass tube using a vortex apparatus. Then, the polycondensation reaction was initiated by adding formic acid to the mixture. After complete addition, the mixture was stirred two minutes until the formation of a homogeneous solution. Monoliths were obtained after 24 hours at room temperature. The exact quantities of the reactants used for the synthesis of

the ionosilica ionogels are given in table 1. The obtained monoliths were kept at 80°C overnight in order to eliminate residual volatiles (HCOOH, HCOOCH$_3$, H$_2$O, CH$_3$OH, etc.). The ionosilica monoliths obtained from TTA, MTTA and TKTA are labelled **TS$_x^{IL}$**, **MT$_x^{IL}$** and **TK$_x^{IL}$** respectively, where x is initial volume of the IL in mL.

Table 1 Used quantities for the synthesis of the ionosilica ionogel materials.

	TTA	IL	FA		MTTA	IL	FA		TKTA	IL	FA
	n(mmol)	n(mmol)	n(mmol)		n(mmol)	n(mmol)	n(mmol)		n(mmol)	n(mmol)	n(mmol)
TS_1^{IL}	6	3	54	MT_1^{IL}	6	3	54	TK_1^{IL}	6	3	72
TS_3^{IL}	6	10	54	MT_3^{IL}	6	10	54	TK_3^{IL}	6	10	72
TS_6^{IL}	6	20	54	MT_6^{IL}	6	20	54	TK_6^{IL}	6	20	72
TS_{12}^{IL}	6	41	54	MT_{12}^{IL}	6	41	54	TK_{12}^{IL}	6	41	72

Solid-state NMR spectroscopy: [1]H solid-state Nuclear Magnetic Resonance NMR spectra were recorded at ν_0 (^{1}H) $\equiv$ 600.1 MHz on a *VARIAN VNMR 600* spectrometer fitted with a Varian HX MAS probe using 3.2 mm ZrO$_2$ rotors. 1D measurements were carried out at 20°C with a $\pi/2$ pulse of 4 μs and a recycling delay of 10 s. The samples were analyzed under MAS at ν_{MAS} = 20 kHz. The chemical shift was referenced using Adamantane as a secondary reference (peak at 1.8 ppm). The acquisition window is 100 kHz and no line broadening has been applied. [1]H transverse relaxation times T_2' were estimated using Hahn echoes with incremented inter-pulse delays.

Raman spectroscopy: Raman measurements were performed on a Fourier transform Raman spectrometer (Bruker RFS100) in the macro configuration with an excitation wavelength of 1064 nm and an impinging power of about 150 mW.

Complex Impedance Spectroscopy (CIS): Impedance measurements were carried out using a Solartron analytical Modulab XM MTS. An *ac* voltage of 20 mV was applied over a frequency domain from f = 1 Hz to f = 1 MHz, at fixed temperature in 273 K – 393 K range. Measurements were carried out with anhydrous solids, after heating the materials at 373 K overnight, followed by several helium purges in order to eliminate residual solvent within the composites. Under these conditions and according to TGA results (figure S7), the solid is fully dehydrated without any traces of formic acid while preventing the IL release. About 75 mg of the powder sample was introduced in a home-made sample holder, *i.e.* between two gold electrodes, in a parallel plate capacitor configuration, with an annular Teflon spacer to avoid short circuits and insure insulation. This configuration corresponds to the basic "two-probe" method for the electrical measurements. The sample surface was deduced from the surface of the smallest electrode, while the sample thickness was evaluated by subtracting the length of the empty sample holder and that of the filled one using a Vernier caliper.

The conductivity was determined considering the value collected at the *dc* plateau in the Bode representation of the real part of the conductivity. Typically, the real part of the *ac* conductivity results from the combination of three contributions:

$$\sigma_{ac}(\omega, T) = \sigma_{MWS}(\omega, T) + \sigma_{dc}(T) + \sigma'(\omega, T) \qquad (1)$$

The polarization component $\sigma'(\omega,T)$, corresponding to the increasing part of the signal at high frequency, arises from the local rearrangement of charges or dipoles causing dipolar reorientation. The dc conductivity plateau $\sigma_{dc}(T)$, resulting from the long-range redistribution of charges dominates the intermediate frequency region. In case of highly ionic conductive materials, the Maxwell Wagner Sillars contribution $\sigma_{MWS}(\omega,T)$ due to the ionic charge accumulation to the sample/electrode interface is observed at low frequency. In insulators, $\sigma_{MWS}(\omega,T) \approx 0$ and $\sigma_{dc}(T) \approx 0$ and only the polarization conductivity is detectable.

Results and Discussion

Our special concern is the design of novel ionogel materials with optimized properties using tailor-made scaffold hosts and IL guests. In this context, we recently reported novel ionosilica ionogels and demonstrated particular confinement effects between an ionosilica host formed from the *tris*-trialkoxysilylated ammonium precursor **TTA** and the ionic liquid [BMIM]TFSI guest in these phases. The material was formed in a straightforward synthesis process only involving the **TTA** precursor, the [BMIM]TFSI IL and formic acid. Under these conditions, the tertiary amine group of the **TTA** precursor is protonated to **H-TTA** and forms ionic ammonium formate entities, simultaneously to the sol-gel process. This feature has been experimentally demonstrated in a previous study.[21] The final material is therefore an ionosilica constituted of ammonium formate groups. As reported before, the confined IL within this ionic host matrix forms two distinct populations: (*i*) the first one interacting with the pore walls *via* electrostatic interactions and (*ii*) the second one, forming bulk-like IL domains.[21]

In this work, we focus on the variation of the host matrix in order to monitor the impact of the constitution of the scaffold on the physico-chemical properties of the ionosilica ionogels materials and in particular on the ion mobility of the confined IL. For this purpose, various ionosilica ionogels were synthesized *via* non-hydrolytic sol-gel procedure from the ionosilica precursors **TTA**, **MTTA** and **TKTA** (Fig. 1) in the presence of variable quantities of the IL [BMIM]TFSI. The conformational change of the ionic species upon confinement is assessed *via* Raman spectroscopy, and the ionic mobilities of the IL are evaluated *via* ^{1}H solid state NMR spectroscopy and Complex Impedance Spectroscopy (CIS) measurements. We determined particularly the mobility of the IL guest as function of (*i*) the molecular structure of the ionosilica host matrix and (*ii*) the amount of the confined IL.

The TFSI anion of the confined IL ([BMIM]TFSI) used in this study is one of the most commonly used anions in ILs. Its flexibility on a molecular scale is reflected by its easy conversion between the *cisoid* and *transoid* conformers displaying C_1 and C_2 symmetry, respectively (Fig. 2). The two conformers present distinct signatures in the Raman spectra in the 250-380 cm^{-1} range.[27] The ratio between the two conformers depends on the local environment and may reflect its direct surroundings on a molecular level, *e.g.* with the ionosilica matrix. Whereas a nearly 1 : 1 ratio between the conformers can be found in the IL bulk,[28] higher C_1/C_2 ratios indicate stronger host-guest interactions. The *cis-trans* ratio of the TFSI anion therefore give an indication between confined and bulk populations of the TFSI anion (Fig. 2).

C$_1$ conformer (*cis*)   C$_2$ conformer (*trans*)
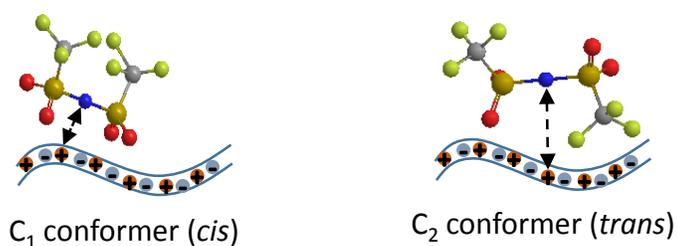
Figure 2 Scheme of the two conformers of the TFSI anion (N: blue, S: orange, O: red, C: grey, F: yellow).

We therefore performed Raman spectroscopy experiments on the ionosilica ionogel composites with the aim to determine the relative proportions of the C_1 and C_2 conformers. The Raman spectra of the **MT$_x^{IL}$** materials (x= 1, 3, 6 and 12) in the 225-425 cm^{-1} range are given in figure 3a, and the Raman spectra of the **TS$_x^{IL}$** and **TK$_x^{IL}$** materials are given in the ESI (figure S4).

The vibrational bands found in the analyzed region can be attributed to the twisting (τ) and rocking (ρ) modes of the SO$_2$ and CF$_3$ groups of the TFSI anion.[29] According to Herstedt *et al.*, the bands at about 306, 326 and 333 cm^{-1} can be used as C_1 indicators, whereas the bands at about 298, 314 and 339 cm^{-1} are characteristic for the C_2 conformer.[28, 30] Although not being a

quantitative method, the deconvolution of the spectra allows the determination of the ratio between the two conformers.[27] The results of the Raman spectra fitting for the materials $\mathbf{MT_x^{IL}}$ (x= 1, 3, 6 and 12) are shown in figure 3b. The contribution of C_1 and C_2 conformers were estimated following the equations 2 and 3:

$$[C_1]= \frac{I_{306}+I_{326}+I_{333}}{\Sigma} \qquad (2)$$

$$[C_2]= \frac{I_{298}+I_{314}+I_{339}}{\Sigma} \qquad (3)$$

Where I_x designates the integrated Raman intensity of a band centered at about wavenumber x and Σ designates the sum of the integrated intensities of all bands at about 298, 306, 314, 326, 333 and 339 cm^{-1}. The relative contributions of the C_1 and C_2 conformers obtained from this procedure for the different ionosilica ionogels are summarized in table 2.

Table 2: Percentage contributions of the two conformers C_1 and C_2 estimated from Raman spectra fitting and using equations (2) and (3).

	C_1(%)	C_2(%)		C_1(%)	C_2(%)		C_1(%)	C_2(%)
TS_1^{IL}	55.0	45.0	MT_1^{IL}	59.0	41.0	TK_1^{IL}	68.5	31.5
TS_3^{IL}	53.0	47.0	MT_3^{IL}	54.0	46.0	TK_3^{IL}	56.0	44.0
TS_6^{IL}	51.0	49.0	MT_6^{IL}	50.5	49.5	TK_6^{IL}	53.0	47.0
TS_{12}^{IL}	49.5	50.5	MT_{12}^{IL}	50.5	49.5	TK_{12}^{IL}	50	50
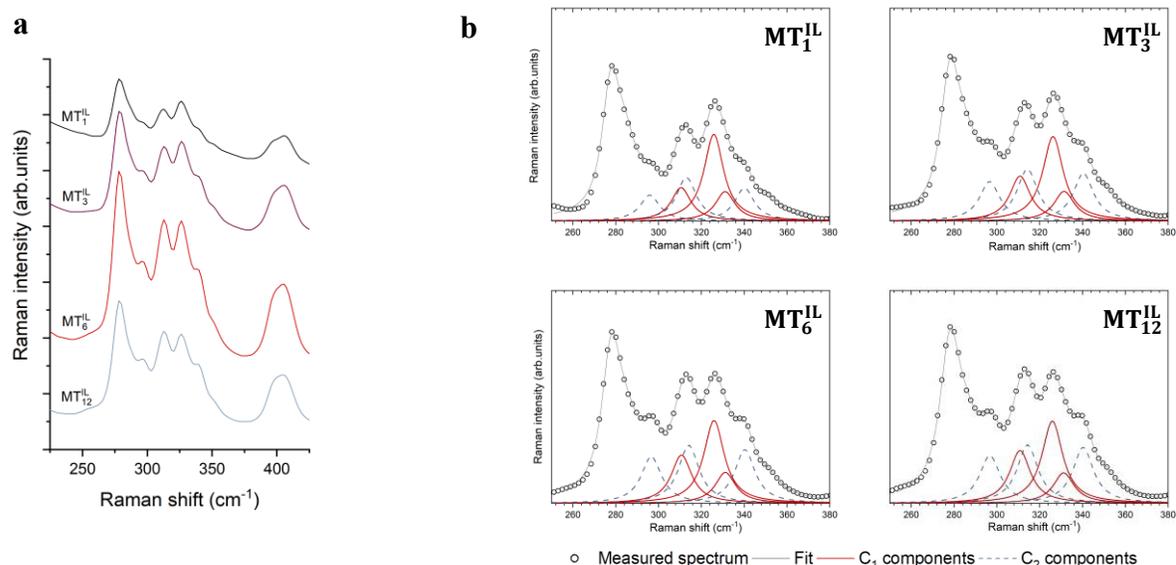
Figure 3 (a) Raman spectra of the $\mathbf{MT_x^{IL}}$ ground monoliths in the range of 225-425 cm^{-1}, (b) Fitted Raman spectra of the $\mathbf{MT_x^{IL}}$ ground monoliths in the 250-380 cm^{-1} range showing the contribution of TFSI anion conformers in the obtained ionosilica ionogels as function of the amount of incorporated IL. Hollow black circles represent experimental data, solid gray line result of the global fit using nine Lorentzian components and red solid (resp. grey dashed) lines highlight the bands attributed to the C_1 (resp. C_2) components.

For the series of ionosilica ionogels $\mathbf{MT_x^{IL}}$, synthesized in the presence of variable amounts of [BMIM]TFSI (x = 1, 3, 6, 12), the C_1 contribution remains always higher than the reference value Th$_1$, that is the C_1 contribution in the bulk IL (49%), whereas the C_2 remains always lower than Th$_2$ (C_2 contribution in the bulk = 51.0%). When the amount of confined IL increases within the material, the C_1 contribution progressively decreases from 59.0% for $\mathbf{MT_1^{IL}}$ to 50.5% for $\mathbf{MT_{12}^{IL}}$. This general increase in the C_1 contribution of the confined TFSI anion with respect to the bulk IL can clearly be associated to the confinement of the IL within the composite, *i.e.* to host guest interactions with the ionosilica matrix. For this reason, the highest contribution of the C_1 conformer was observed with the material containing the lowest amount of IL ($\mathbf{MT_1^{IL}}$), and

16

almost reaches the value observed in the bulk for the material synthesized with the highest IL quantities ($\mathbf{MT_{12}^{IL}}$). The increase of the contribution of the C_2 conformer can therefore be attributed to an enhancement of the bulk fraction of the confined IL. Similar trends are observed for $\mathbf{TS_x^{IL}}$ and $\mathbf{TK_x^{IL}}$ materials.
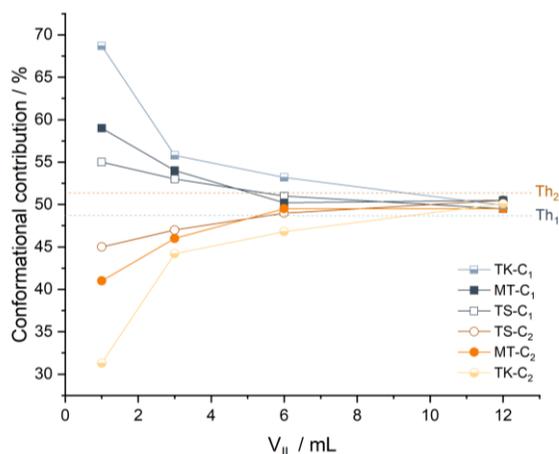
Figure 4 Relative contributions of TFSI C_1 and C_2 conformers estimated using the analysis of the Raman spectra (see main text) in the obtained ionosilica ionogels as function of the incorporated IL amount and the molecular structure of ionosilica matrix

Furthermore, a clear impact of the nature of the ionosilica matrix on the C_1/C_2 ratio could also be observed. For a similar amount of incorporated IL (*e.g.* 1 mL), the material synthesized using the **TKTA** precursor shows the highest contribution of the C_1 conformer (68.5 %) compared to the one obtained from the **MTTA** and the **TTA** precursors (59.0 and 55.0 %, respectively). This trend that was also observed in the series of materials synthesized in the presence of 3 and 6 mL of IL, points more pronounced host-guest interactions in the materials obtained from the **TKTA** and **MTTA** precursors. The effect attenuates in the materials synthesized in the presence of 12 mL, where the C_1/C_2 ratio almost reaches the value observed in the bulk IL whatever the

ionosilica matrix (figure 4). The observed increase of the C_1 conformational contribution reflects increasing host-guest interactions in the series of the materials $\textbf{TS}_\textbf{x}^\textbf{IL} < \textbf{MT}_\textbf{x}^\textbf{IL} < \textbf{TK}_\textbf{x}^\textbf{IL}$. The reduced IL-scaffold interactions in the case of $\textbf{TS}_\textbf{x}^\textbf{IL}$ may be attributed to a larger "accessible-IL" volume (*i.e.* less reticulated network) and thus to a lower surface-bounded/ bulk-like IL populations ratio, whereas the IL in the case of $\textbf{TK}_\textbf{x}^\textbf{IL}$, the materials undergo stronger confinement effects due to the presence of a fourth crosslinking knot within the ionic building blocks. $\textbf{MT}_\textbf{x}^\textbf{IL}$ Materials show intermediate behavior explained by the substitution of the proton ($\textbf{TS}_\textbf{x}^\textbf{IL}$) by a more bulky methyl group (figure 1).

To confirm these results, we have also carried out the analysis of the Raman spectra following the approach reported by Wu *et al.* .[31] These authors used the bands at about 312, 326 and 405 cm^{-1} and about 295, 339 and 396 cm^{-1} to reveal the ratios between the C_1 and the C_2 conformer (figures S4-S5 and table S1). The trends observed regarding the evolution of the C_1/C_2 ratio as a function of the ionosilica scaffold and the IL content of the materials are coherent with the analysis discussed before (*vide supra*). Raman spectroscopy therefore gives a clear indication for the evolution of the C_1/C_2 conformer ratio, and also reveals significant differences between the three investigated host matrices, thus highlighting modulable host-guest interactions in these systems.

To further investigate the IL confinement effect within the ionosilica host matrix, ^{1}H solid-state NMR spectroscopy experiments were performed. The ^{1}H MAS NMR spectra of the ground $\textbf{MT}_\textbf{x}^\textbf{IL}$ monoliths are represented in figure 5a. All spectra show the characteristic signals of the imidazolium cation with highly variable peak widths and overlapping the broader peaks of the $\textbf{MT}$ matrix. The full width at half maximum (FWHM) value of all peaks decreases gradually

when the concentration of the IL increases.[32-33] Similar results were observed for all ionosilica ionogel materials TS_x^{IL} and TK_x^{IL} (figure S6).

The observed decrease in the FWHM of the peaks is a direct response to the dynamics of the mobile liquid phase within the solid matrix.[34] Therefore, in order to obtain further insight in the mobility of the confined IL, we determined the average transverse relaxation times T_2' of imidazolium ^1H signals from spin echo decays. The spin echo NMR sequence measures an exponential decay known as the relaxation time T_2' by acquiring the NMR signals for different spacing of the two pulses (echo time). The ^1H T_2' values of the -C^1H and –C^5H located at 0.7 ppm and 7.3 ppm are summarized in table S2 (ESI). The evolution of the T_2' values as function of the volume of the IL and the nature of the ionosilica scaffold is represented in figure 5b.
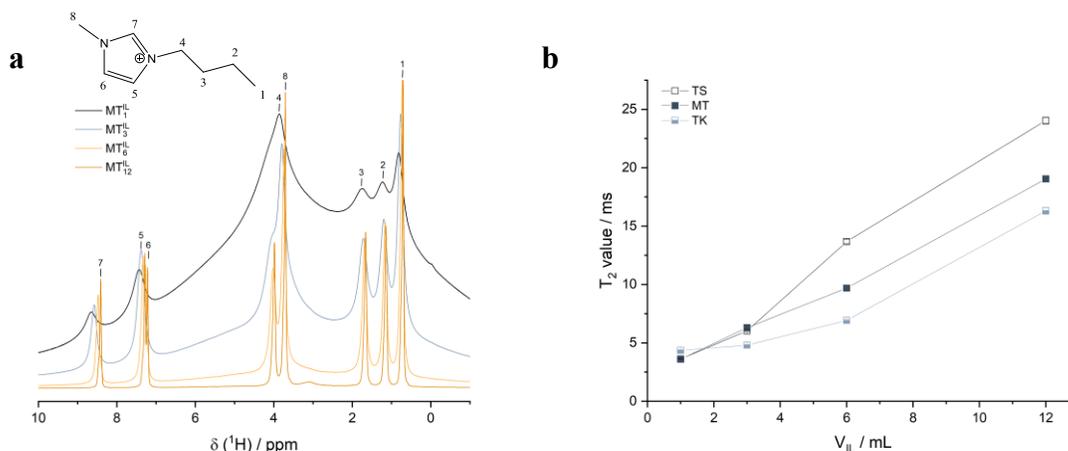
Figure 5 (a) ^1H solid-state MAS NMR spectra of ground MT_x^{IL} monoliths (ν_{MAS} = 20 kHz) and (b) T_2'values as function of the volume of the IL of the different ionosilica ionogels for the peak at 0.7 ppm.

Our results show that the T_2' values gradually increases with the increase in the amount of confined IL for all ionosilica ionogels, as for example from 3.6 ms for MT_1^{IL} to 19.0 ms for MT_{12}^{IL}

for the materials obtained from the **MTTA** precursor. The obtained results are in accordance with the decrease in the FWHM observed in ^{1}H solid-state MAS spectra. Higher T_2' values therefore suggest increasing mobilities of the confined IL (*vide infra*). On the other side, the T_2' values also depend on the ionosilica matrix. Generally speaking, the T_2' values are the highest in the materials constituted of a **TS** matrix and the lowest in the materials based on a **TK** matrix. For example, for the materials synthesized in the presence of 6 mL of IL using the different ionosilica precursors, the T_2' value decreases from 13.7 ms for the material $\mathbf{TS_6^{IL}}$ to 9.7 ms for material $\mathbf{MT_6^{IL}}$ to reach a minimum value of 6.9 ms for $\mathbf{TK_6^{IL}}$ material. This trend can be observed for all other series of ionosilica ionogel materials synthesized with different amounts of IL.

The large variations in T_2' observed as function of the amount of confined IL or the nature of the scaffold can be related to variations in effective homonuclear ^{1}H-^{1}H dipolar couplings D_{HH}, here the main contributions to transverse relaxation mechanism. Therefore, the increase in T_2' is related to a decrease in D_{HH} that can be explained by increased degrees of motion for the IL. These findings elucidate the imidazolium cation dynamics relatively to the amount of the confined IL and the nature of the ionosilica scaffold and are in line with the results obtained in Raman experiments. Furthermore, the observed results suggest the presence of a labile proton, enhancing the mobility of the confined IL in the case of $\mathbf{TS_x^{IL}}$**.** The protonation of the ionosilica matrix in the case of $\mathbf{TS_x^{IL}}$ or an interaction between the IL and the (N-H) group might yield additional H$^+$ ions that contribute to the increased IL dynamics. Whereas $\mathbf{TK_x^{IL}}$ being constituted of tetraalkylammonium building blocks undergo a decrease in the IL mobility due the increased crosslinking within the network.

The electrical properties of the pure ionosilica matrices and the corresponding composites were evaluated by CIS. As illustrated in figure S8, the Bode representation of the conductivity for the pure TS ionosilica matrix is dominated by the polarization conductivity, resulting from the dipolar relaxation of polar components of the polymer. The very low conductivity values coupled with the absence of the *dc* conductivity contribution indicates that **TS** matrix is an insulator, suggesting that the formate species cannot diffuse over long distances without the assistance of guest charge carriers. For the **MT** and **TK** ionosilica matrices, conductivity values are at least one order of magnitude higher compared to that recorded on **TS**, while remaining very low. Accordingly, the *dc* conductivity response is only observable at temperature higher than 343 K and 363 K for **MT** (figure S8) and **TK** (figure S9) matrices respectively. This trend evidences that iodide ions are slightly more mobile than formate species, even though they still require guest species to be efficiently transported within the **MT** and **TK** matrices.

On the opposite, the $\sigma_{ac}(\omega)$ profile drastically changes for the composites (see figures S11-S13). The $\sigma_{ac}(\omega)$ spectra exhibit Maxwell-Wagner Sillars, *dc* and polarization conductivity contributions for $\mathbf{TS^{IL}_{12}}$ and $\mathbf{MT^{IL}_{6}}$, while the Maxwell-Wagner Sillars contribution is missing for $\mathbf{TK^{IL}_{1}}$, in agreement with the lower conductivity displayed by this composite. The diffusion conductivity plateau observed once the IL is incorporated inside the ionosilica matrix underlines that σ_{dc} is assigned to the IL dynamics. IL participates to the conductivity process as a charge carrier and by providing additional ions.[35-36]
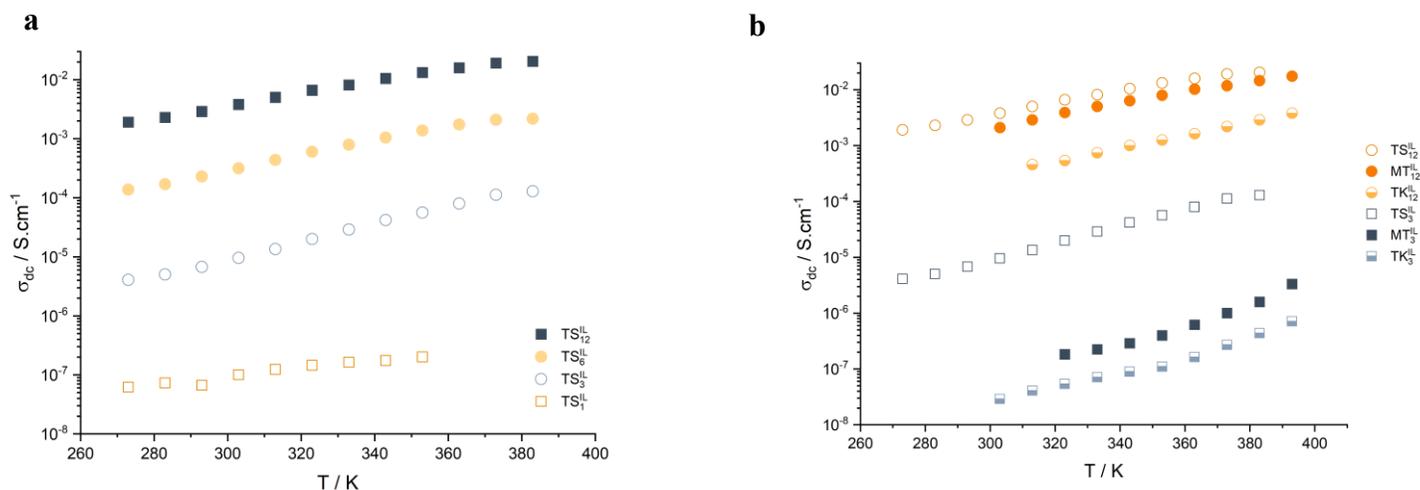
Figure 6 (a) Temperature dependence of the *dc* conductivity for the ionosilica ionogels synthesized using **TTA** precursor in the presence of variable amount of [BMIM]TFSI. (b) Temperature dependence of the *dc* conductivity for the ionosilica ionogels synthesized in the presence of variable amount of [BMIM]TFSI

The *dc* conductivity values were then evaluated in the frequency independent domain of $\sigma_{ac}(\omega)$ at each temperature and further discussed according to the IL content and the ionosilica nature. For the TS_x^{IL} series of ionosilica ionogels synthesized in the presence of variable amounts of [BMIM]TFSI (x = 1, 3, 6, 12) (figure 6a), the *dc* conductivity is boosted with increasing the IL content, *i.e.* with increasing the charge carriers concentration. Accordingly, TS_{12}^{IL} displays the best performances: its σ_{dc} values are four orders of magnitude higher than those recorded for TS_1^{IL}. The raise of the conductivity with IL increase is also observed for both other series of ionosilicas (see figures S14 and S15). It relies on the monotonous change of the ratio between the two guest populations while increasing the IL concentration.[21, 35, 37] The first one refers to the interfacial layer composed of ILs interacting with the pore walls *via* electrostatic interactions, which prevails at low IL concentration. This host-guest interaction makes the dynamics of the

system slowed down because of the dominating population of IL in *cis* conformation, as evidenced in Raman spectroscopy.[27, 34] The second population which becomes significant at high IL loading, is associated with the bulk-like IL population localized in the center of the porosity. Compared to the IL population interacting with the pore walls, the viscosity of the system decreases and merge toward that of the bulk IL, improving the dynamics of the system, as reported for composites resulting from ILs supported in various porous solids.[38-43] As a support, the conductivity of $\textbf{TS}_{\textbf{12}}^{\textbf{IL}}$ recorded at 333 K (σ_{dc} = 8.13 x 10^{-3} S.cm^{-1}, see Table 3) is consistent with the value reported for the bulk [BMim]TFSI (σ_{dc} = 8.00 x 10^{-3} S.cm^{-1}).[44]

In addition, the electrical properties of the ionosilica ionogels are equally impacted by the nature of the ionosilica precursor. At fixed IL content, the conductivity performance of the composites follows the $\textbf{TS}_{\textbf{x}}^{\textbf{IL}}$ > $\textbf{MT}_{\textbf{x}}^{\textbf{IL}}$ > $\textbf{TK}_{\textbf{x}}^{\textbf{IL}}$ sequence (see Figure 6b). This sequence remains valid whatever the IL concentration, x, and further agrees with the conclusions deduced from NMR and Raman analysis. It evidences specific (*i*) host/guest interactions and/or (*ii*) typical conduction pathways for the charge carriers diffusion within the host matrix according to the ionosilica precursor. Noteworthy, the $\textbf{TK}_{\textbf{x}}^{\textbf{IL}}$ series displays the lowest conductivity values, in relation with the four cross-linking knots involved in the **TKTA** precursor, which makes the polymer highly rigid and further impedes the movements of the guest species. On the opposite, the high conductivity values recorded on the $\textbf{TS}_{\textbf{X}}^{\textbf{IL}}$ composites reveals that the pathway for the ions transfer inside the polymeric host is favored by the less steric **H-TTA** precursor, creating free volume large enough to achieve less constrained dynamics of the IL than in $\textbf{TK}_{\textbf{x}}^{\textbf{IL}}$. Based on this, $\textbf{MT}_{\textbf{x}}^{\textbf{IL}}$ composites show an intermediate behavior, in relation with the bulkier methyl group of **MTTA** replacing the hydrogen of (N-H) groups of the **H-TTA** precursor of the $\textbf{TS}_{\textbf{X}}^{\textbf{IL}}$ series. In the case of $\textbf{TS}_{\textbf{X}}^{\textbf{IL}}$, one also notes that the interaction between IL and the (N-H) group of the **H-**

TTA precursor might also produce additional H$^+$ ions that could participate to the ion conduction process,[45] magnifying the conductivity performances recorded on this series of composites.

Table 3: Diffusion conductivity values recorded at 333 K for the $\mathbf{TS_x^{IL}}$, $\mathbf{MT_x^{IL}}$ and $\mathbf{TK_x^{IL}}$ series of ionosilica ionogels.

	σ_{dc} (S.cm^{-1})		σ_{dc} (S.cm^{-1})		σ_{dc} (S.cm^{-1})
$\mathbf{TS_1^{IL}}$	1.62×10^{-7}	$\mathbf{MT_1^{IL}}$	5.08×10^{-9}	$\mathbf{TK_1^{IL}}$	5.25×10^{-10}
$\mathbf{TS_3^{IL}}$	2.88×10^{-5}	$\mathbf{MT_3^{IL}}$	2.23×10^{-7}	$\mathbf{TK_3^{IL}}$	7.07×10^{-8}
$\mathbf{TS_6^{IL}}$	7.94×10^{-4}	$\mathbf{MT_6^{IL}}$	5.25×10^{-5}	$\mathbf{TK_6^{IL}}$	2.75×10^{-5}
$\mathbf{TS_{12}^{IL}}$	8.13×10^{-3}	$\mathbf{MT_{12}^{IL}}$	5.01×10^{-4}	$\mathbf{TK_{12}^{IL}}$	7.41×10^{-4}

Conclusion

In this work, we investigated the influence of (*i*) the nature of the ionosilica scaffold and the (*ii*) ionosilica/IL ratio on the mobility of the confined IL. Therefore, various ionosilica ionogel composites were synthesized evolving three different ionosilica precursors with different amounts of confined IL. Three characterization techniques were used to elucidate the host-guest interactions and thus the IL dynamics within the systems: Raman spectroscopy, ^{1}H solid-state NMR and Complex Impedance Spectroscopies.

Raman experiments reveal stronger host/guest interactions in the $\mathbf{TK_x^{IL}}$ materials compared to the $\mathbf{TS_x^{IL}}$ ones due to a higher crosslinking degree in the latter. Furthermore, significant increase in the *transoid* form was noticed relative to the decrease in the host/guest ratio. This increase reflects a reduce host-guest interactions with the increase in *bulk-like IL fraction* within the ionosilica scaffold. Concomitantly, ^{1}H solid-state spin echo NMR and CIS measurements suggest that the IL dynamics within composites is strongly dependent of the scaffold nature and the host/guest ratio. At fixed IL content, the IL dynamics within the network follows the $\mathbf{TS_x^{IL}}$ > $\mathbf{MT_x^{IL}}$ > $\mathbf{TK_x^{IL}}$ sequence. The observed result can be explained by (*i*) the existence of a labile (N-H) proton in the case of $\mathbf{TS_x^{IL}}$ which may create additional charge carriers contributing to the increased conductivity of the system and (*ii*) the presence of a fourth crosslinking knot in the case of $\mathbf{TK_x^{IL}}$ composites impeding the local movement of the mobile guest species. Additionally, the results show an increase in the IL dynamics with the decrease in the ionosilica content relative to the increase in the bulk-like IL population within the network. Accordingly, the dynamics of IL in $\mathbf{TS_{12}^{IL}}$ reaches that of the bulk demonstrating the particular confinement of the IL within the ionosilica matrix which allows the preservation of the IL properties while trapped within a solid scaffold.

25

This possibility to significantly enhance the ionic mobility by tuning the nature of ionosilica scaffold and the amount confined IL highlights the unique and interesting properties of ionosilica ionogel composites. These designer solid materials may be of high interest for many applications in different fields, *e.g.* as solid electrolyte in the energy storage domain.

Supporting Information

Electronic supplementary information (ESI) available. See DOI: XXX

- Ionosilica precursors detailed synthesis.

- Liquid NMR spectra of the ionosilica precursors.

- Supplementary Raman spectra for $\mathbf{TS_x^{IL}}$ and $\mathbf{TK_x^{IL}}$.

- C_1/C_2 conformers contribution following the approach reported by Wu *et al.*.[31]

- ^{1}H NMR MAS spectra of $\mathbf{TS_x^{IL}}$ and $\mathbf{TK_x^{IL}}$ monoliths.

- TGA curve of $\mathbf{MT_6^{IL}}$ monolith after 12 hours at 100°C.

- Supplementary Bode representation of the conductivity in the 273 K- 393 K temperature range.

- Supplementary temperature dependence of the *dc* conductivity for $\mathbf{TS_x^{IL}}$ and $\mathbf{TK_x^{IL}}$ monoliths.

Author Contributions

The manuscript was written through contributions of all authors. All authors have given approval to the final version of the manuscript.

Notes

The authors declare no competing financial interest.

References

1.   Watanabe, M.; Thomas, M. L.; Zhang, S.; Ueno, K.; Yasuda, T.; Dokko, K., Application of Ionic Liquids to Energy Storage and Conversion Materials and Devices. *Chemical Reviews* **2017,** *117* (10), 7190.
2.   Pârvulescu, V. I.; Hardacre, C., Catalysis in Ionic Liquids. *Chemical Reviews* **2007,** *107* (6), 2615.
3.   Hallett, J. P.; Welton, T., Room-Temperature Ionic Liquids: Solvents for Synthesis and Catalysis. 2. *Chemical Reviews* **2011,** *111* (5), 3508.
4.   Hasib-ur-Rahman, M.; Siaj, M.; Larachi, F., Ionic liquids for CO2 capture—Development and progress. *Chemical Engineering and Processing: Process Intensification* **2010,** *49* (4), 313.
5.   Shiflett, M. B., *Commercial Applications of Ionic Liquids*. 1st ed. 2020 édition (14 février 2021) ed.; 2020.
6.   Le Bideau, J.; Viau, L.; Vioux, A., Ionogels, ionic liquid based hybrid materials. *Chemical Society Reviews* **2011,** *40* (2), 907.
7.   Susan, M. A.; Kaneko, T.; Noda, A.; Watanabe, M., Ion gels prepared by in situ radical polymerization of vinyl monomers in an ionic liquid and their characterization as polymer electrolytes. *Journal of the American Chemical Society* **2005,** *127* (13), 4976.
8.   Tome, L. C.; Porcarelli, L.; Bara, J. E.; Forsyth, M.; Mecerreyes, D., Emerging iongel materials towards applications in energy and bioelectronics. *Materials Horizons* **2021,** *8* (12), 3239.
9.   Taylor, M. E.; Panzer, M. J., Fully-Zwitterionic Polymer-Supported Ionogel Electrolytes Featuring a Hydrophobic Ionic Liquid. *Journal of Physical Chemistry B* **2018,** *122* (35), 8469.
10.   Nguyen, T. P.; Hesemann, P.; Tran, T. M. L.; Moreau, J. J. E., Nanostructured polysilsesquioxanes bearing amine and ammonium groups by micelle templating using anionic surfactants. *Journal of Materials Chemistry* **2010,** *20* (19), 3910.
11.   Rodrigues, A. D.; Jacob, M.; Gauchou, V.; Durand, J.-O.; Trens, P.; Prelot, B.; Hesemann, P., Controlled synthesis and osmotic properties of ionosilica nanoparticles. *Microporous and Mesoporous Materials* **2021,** *310*, 110644.
12.   Sauvanier, D.; Li, W. S. J.; Ferlin, N.; Lacroix-Desmazes, P.; Prelot, B.; Hesemann, P., Simple and Straightforward Synthesis of Porous Ionosilica for Efficient Chromate Adsorption. *Israel Journal of Chemistry* **2019,** *59* (9), 843.
13.   Thach, U. D.; Hesemann, P.; Yang, G. Z.; Geneste, A.; Le Caer, S.; Prelot, B., Ionosilicas as efficient sorbents for anionic contaminants: Radiolytic stability and ion capacity. *Journal of Colloid and Interface Science* **2016,** *482*, 233.
14.   Bouchal, R.; Miletto, I.; Thach, U. D.; Prelot, B.; Berlier, G.; Hesemann, P., Ionosilicas as efficient adsorbents for the separation of diclofenac and sulindac from aqueous media. *New Journal of Chemistry* **2016,** *40* (9), 7620.
15.   Thach, U. D.; Prelot, B.; Pellet-Rostaing, S.; Zajac, J.; Hesemann, P., Surface Properties and Chemical Constitution as Crucial Parameters for the Sorption Properties of Ionosilicas: The Case of Chromate Adsorption. *ACS Applied Nano Materials* **2018,** *1* (5), 2076.
16.   Bouchal, R.; Daurat, M.; Gary-Bobo, M.; Da Silva, A.; Lesaffre, L.; Aggad, D.; Godefroy, A.; Dieudonne, P.; Charnay, C.; Durand, J. O*., et al.*, Biocompatible Periodic Mesoporous Ionosilica Nanoparticles with Ammonium Walls: Application to Drug Delivery. *ACS Applied Materials & Interfaces* **2017,** *9* (37), 32018.

17.   Daurat, M.; Rahmani, S.; Bouchal, R.; Akrout, A.; Budimir, J.; Nguyen, C.; Charnay, C.; Guari, Y.; Richeter, S.; Raehm, L.*, et al.*, Organosilica Nanoparticles for Gemcitabine Monophosphate Delivery in Cancer Cells. *ChemNanoMat* **2019,** *5* (7), 888.

18.   Mezghrani, B.; Ali, L. M. A.; Richeter, S.; Durand, J. O.; Hesemann, P.; Bettache, N., Periodic Mesoporous Ionosilica Nanoparticles for Green Light Photodynamic Therapy and Photochemical Internalization of siRNA. *ACS Applied Materials & Interfaces* **2021,** *13* (25), 29325.

19.   Hesemann, P.; Nguyen, T. P.; El Hankari, S., Precursor Mediated Synthesis of Nanostructured Silicas: From Precursor-Surfactant Ion Pairs to Structured Materials. *Materials* **2014,** *7* (4), 2978.

20.   Thach, U. D.; Trens, P.; Prelot, B.; Zajac, J.; Hesemann, P., Tuning the Interfacial Properties of Mesoporous Ionosilicas: Effect of Cationic Precursor and Counter Anion. *Journal of Physical Chemistry C* **2016,** *120* (48), 27412.

21.   Abdou, N.; Landois, P.; Brun, N.; Alonso, B.; Taubert, A.; Hesemann, P.; Mehdi, A., Ionic Guest in Ionic Host: Ionosilica Ionogel Composites via Ionic Liquid Confinement in Ionosilica Supports. *Materials Chemistry Frontiers* **2022,** *6*, 939.

22.   Sharp, K. G., A Two-Component, Non-Aqueous Route to Silica Gel. *Journal of Sol-Gel Science and Technology* **1994,** *2* (1-3), 35.

23.   Dai, S.; Ju, Y. H.; Gao, H. J.; Lin, J. S.; Pennycook, S. J.; Barnes, C. E., Preparation of silica aerogel using ionic liquids as solvents. *Chemical Communications* **2000,** (3), 243.

24.   Martinelli, A.; Nordstierna, L., An investigation of the sol-gel process in ionic liquid-silica gels by time resolved Raman and H-1 NMR spectroscopy. *Physical Chemistry Chemical Physics* **2012,** *14* (38), 13216.

25.   Viau, L.; Neouze, M. A.; Biolley, C.; Volland, S.; Brevet, D.; Gaveau, P.; Dieudonne, P.; Galarneau, A.; Vioux, A., Ionic Liquid Mediated Sol-Gel Synthesis in the Presence of Water or Formic Acid: Which Synthesis for Which Material? *Chemistry of Materials* **2012,** *24* (16), 3128.

26.   Nguyen, T. P.; Hesemann, P.; Linh Tran, T. M.; Moreau, J. J. E., Nanostructured polysilsesquioxanes bearing amine and ammonium groups by micelle templating using anionic surfactants. *Journal of Materials Chemistry* **2010,** *20* (19), 3910.

27.   Martinelli, A.; Matic, A.; Johansson, P.; Jacobsson, P.; Borjesson, L.; Fernicola, A.; Panero, S.; Scrosati, B.; Ohno, H., Conformational evolution of TFSI- in protic and aprotic ionic liquids. *Journal of Raman Spectroscopy* **2011,** *42* (3), 522.

28.   Herstedt, M.; Smirnov, M.; Johansson, P.; Chami, M.; Grondin, J.; Servant, L.; Lassegues, J. C., Spectroscopic characterization of the conformational states of the bis (trifluoromethanesulfonyl)imide anion (TFSI⁻). *Journal of Raman Spectroscopy* **2005,** *36* (8), 762.

29.   Rey, I.; Johansson, P.; Lindgren, J.; Lassegues, J. C.; Grondin, J.; Servant, L., Spectroscopic and theoretical study of $(CF_3SO_2)(2)N^-$ (TFSI⁻) and $(CF_3SO_2)(2)NH$ (HTFSI). *Journal of Physical Chemistry A* **1998,** *102* (19), 3249.

30.   Martinelli, A., Conformational Changes and Phase Behaviour in the Protic Ionic Liquid 1-Ethylimidazolium Bis(trifluoromethylsulfonyl)imide in the Bulk and Nano-Confined State. *European Journal of Inorganic Chemistry* **2015,** (7), 1300.

31.   Wu, J.; Zhu, X.; Li, H. N.; Su, L.; Yang, K.; Cheng, X. R.; Yang, G. Q.; Liu, J., Combined Raman Scattering and X-ray Diffraction Study of Phase Transition of the Ionic Liquid BMIM TFSI Under High Pressure. *Journal of Solution Chemistry* **2015,** *44* (10), 2106.

32.   Echelmeyer, T.; Meyer, H. W.; van Wullen, L., Novel Ternary Composite Electrolytes: Li Ion Conducting Ionic Liquids in Silica Glass. *Chemistry of Materials* **2009,** *21* (11), 2280.

33.   Noda, A.; Hayamizu, K.; Watanabe, M., Pulsed-gradient spin-echo H-1 and F-19 NMR ionic diffusion coefficient, viscosity, and ionic conductivity of non-chloroaluminate room-temperature ionic liquids. *Journal of Physical Chemistry B* **2001,** *105* (20), 4603.

34.   Nayeri, M.; Aronson, M. T.; Bernin, D.; Chmelka, B. F.; Martinelli, A., Surface effects on the structure and mobility of the ionic liquid C(6)C(1)ImTFSI in silica gels. *Soft Matter* **2014,** *10* (30), 5618.

35.   Iacob, C.; Sangoro, J. R.; Kipnusu, W. K.; Valiullin, R.; Karger, J.; Kremer, F., Enhanced charge transport in nano-confined ionic liquids. *Soft Matter* **2012,** *8* (2), 289.

36.   Neouze, M. A.; Le Bideau, J.; Leroux, F.; Vioux, A., A route to heat resistant solid membranes with performances of liquid electrolytes. *Chemical Communications* **2005,** (8), 1082.

37.   Vioux, A.; Coasne, B., From Ionogels to Biredox Ionic Liquids: Some Emerging Opportunities for Electrochemical Energy Storage and Conversion Devices. *Advanced Energy Materials* **2017,** *7* (22), 1700883.

38.   MacFarlane, D. R.; Forsyth, M.; Howlett, P. C.; Kar, M.; Passerini, S.; Pringle, J. M.; Ohno, H.; Watanabe, M.; Yan, F.; Zheng, W. J.*, et al.*, Ionic liquids and their solid-state analogues as materials for energy generation and storage. *Nature Reviews Materials* **2016,** *1* (2), 15005.

39.   Le Bideau, J.; Gaveau, P.; Bellayer, S.; Neouze, M. A.; Vioux, A., Effect of confinement on ionic liquids dynamics in monolithic silica ionogels: H-1 NMR study. *Physical Chemistry Chemical Physics* **2007,** *9* (40), 5419.

40.   Singh, M. P.; Singh, R. K.; Chandra, S., Ionic liquids confined in porous matrices: Physicochemical properties and applications. *Progress in Materials Science* **2014,** *64* (Complete), 73.

41.   Noor, S. A. M.; Bayley, P. M.; Forsyth, M.; MacFarlane, D. R., Ionogels based on ionic liquids as potential highly conductive solid state electrolytes. *Electrochimica Acta* **2013,** *91*, 219.

42.   Guyomard-Lack, A.; Delannoy, P. E.; Dupre, N.; Cerclier, C. V.; Humbert, B.; Le Bideau, J., Destructuring ionic liquids in ionogels: enhanced fragility for solid devices. *Physical Chemistry Chemical Physics* **2014,** *16* (43), 23639.

43.   Yoshida, Y.; Fujie, K.; Lim, D. W.; Ikeda, R.; Kitagawa, H., Superionic Conduction over a Wide Temperature Range in a Metal-Organic Framework Impregnated with Ionic Liquids. *Angewandte Chemie-International Edition* **2019,** *58* (32), 10909.

44.   Vranes, M.; Dozic, S.; Djeric, V.; Gadzuric, S., Physicochemical Characterization of 1-Butyl-3-methylimidazolium and 1-Butyl-1-methylpyrrolidinium Bis(trifluoromethylsulfonyl)imide. *Journal of Chemical and Engineering Data* **2012,** *57* (4), 1072.

45.   Vavra, S.; Elamin, K.; Evenas, L.; Martinelli, A., Transport Properties and Local Structure of an Imidazole/Protic Ionic Liquid Mixture Confined in the Mesopores of Hydrophobic Silica. *Journal of Physical Chemistry C* **2021,** *125* (4), 2607.